The Influence of Hydrobionts on Net Construction

Alexander Nedostup, Alexey Razhev, Pavel Nasenkov, and Karina Konovalova(✉)

Kaliningrad State Technical University, 1, Sovetsky Avenue, Kaliningrad 236022, Russian Federation
karina.konovalova@klgtu.ru

Abstract. The study investigates the influence of hydrodynamic backwater on trawl cod-end performance. Conventional biomass-assessment models fall short in open-water fisheries, leading to the adoption of hydrodynamic backwater as a critical variable affecting catch-efficiency. A numerical framework grounded in Navier-Stokes equations and the vorticity-stream function (ω-ψ) formulation is constructed to simulate cod-end flows under varying design parameters – including inlet diameter, mesh spacing, mesh orientation, and trawling speed. Experimental simulations identify optimal geometries that minimize hydrodynamic backwater and maximize catch-efficiency. Findings reveal that a reduced inlet diameter and mesh spacing combined with a T90 mesh orientation cut hydrodynamic backwater by 15–20%. Hydrodynamic backwater escalates sharply at higher trawling speeds, diminishing efficiency; the optimal speed window is 1.5–2.5 m/s. The ω-ψ solutions closely match hydro-channel experimental data, validating the model's accuracy. These results emphasize the necessity of incorporating hydrodynamic backwater considerations into net design and provide concrete recommendations for structural optimization to improve trawl performance. Future work should explore adaptive mesh configurations that respond to real-time hydrodynamic conditions, integrating machine-learning algorithms to predict optimal mesh spacing and orientation, thereby further reducing hydrodynamic backwater and enhancing selectivity while maintaining high catch rates across diverse pelagic species.

Keywords: Hydrodynamic Backwater · Trawl Cod-End · Catch-Efficiency Coefficient · Navier–Stokes Equations · Numerical Simulation

1 Introduction

The modern state of assessing the biomass of marine aquatic organism in the World Ocean relies on mathematical and instrumental methods for determining the parameters of aquatic biological resource stocks. Mathematical models have proven effective in closed water bodies, but their applicability in open ocean conditions is limited due to the large number of parameters involved in the behavioral equations of hydrobionts. Conversely, instrumental methods demonstrate high accuracy in open water bodies, yet they require known values of catch-efficiency coefficients of fishing gear.

© The Author(s), under exclusive license to Springer Nature Switzerland AG 2027
A. Ronzhin et al. (Eds.): ADOP 2026, SIST 508, pp. 439–448, 2027.
https://doi.org/10.1007/978-3-032-35010-7_35

In our case, the catch-efficiency coefficient of a trawl depends on many parameters. It reflects the effectiveness of the fishing gear relative to the actual abundance of fish or their availability at a given location; it indicates what proportion of fish entering the trawling area are actually retained, and it is used to assess aquatic biological resource stocks and the effort required for fishing. This coefficient is calculated from catch statistics and fishes school data, helping to evaluate the accuracy of «catch» from the school of fishes [1–3].

The behavioral characteristics of hydrobionts in the trawl area vary among each other. In the inlet part, they are one set of parameters, while in the terminal part they are different, most clearly expressed when considering the hydrodynamic backwater generated in the trawl area (Fig. 1).

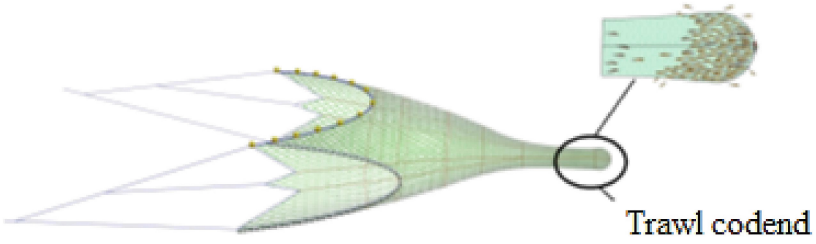

Fig. 1. Multi-depth trawl

The problem of influencing the behavioral characteristics of hydrobionts in the trawling area, when flows are strong and there is a large difference in velocity and pressure fields inside and outside the trawling area, can be addressed using the Navier-Stokes equations.

2 Hydrodynamic Backwater in the Trawling Area

Hydrodynamic backwater in the trawling area arises from pressure differences. In this case, the larger the hydrodynamic backwater, the more difficult it is for fish to enter the trawl net, and consequently the catch-efficiency coefficient of the trawl – a measurable quantity – will not give an accurate value when determining hydrobionts stocks (Fig. 2).

The magnitude of hydrodynamic backwater in the trawl net significantly affects the catch-efficiency coefficient of the trawl. This parameter must not be underestimated when assessing the trawl catch-efficiency. Hydrodynamic backwater is influenced by factors such as the diameter of the inlet mouth of the cod-end, the net itself, the diameter of the rope or cord from which the cod-end and the trawl net are made, the mesh size and its orientation (T0 or T90), the length of the trawl net, the net's belt, the presence of a sleeve and frame, and the trawling speed. Moreover, when the trawling speed is high, the hydrodynamic backwater increases, reducing the trawling speed; the catch-efficiency coefficient can drop sharply due to fish escape from the trawl. Thus, the relationship between catch-efficiency and hydrodynamic backwater allows the determination of optimal trawling conditions and the achievement of high trawl catch-efficiency values [4–9].

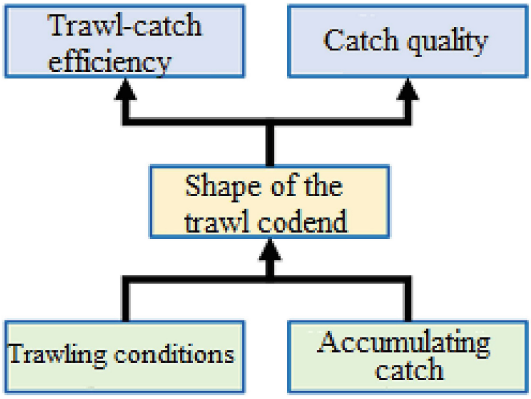

Fig. 2. Influence on trawl catch-efficiency

3 Proposed Approach

Based on the software «Hydrodynamics of the Trawl cod-end» we calculated the shape of the cod-end and the loads on its elements for various design parameters of the cod-end, trawling speed, and mesh orientation, followed by visualization in three-dimensional, two-dimensional and numerical representations.

For the numerical experiment a trawl cod-end with the following design characteristics (shown in Table 1) was selected.

Table 1. Design characteristics of the trawl cod-end

№	Parameter	Designation	Value
1	Number of mesh along the axis of the net structure	m	20
2	Number of mesh along the circumference of the net structure	n	10
3	Diameter of the left row	D	50,0 mm
4	Diameter	d	2,0 mm
5	Thickening coefficient of the node	k_y	3
6	Mesh pitch	a	20 mm

Parameters of external influence show in Table 2.

When specifying the node diameter, the thickening coefficient: $k_y = d_n/d$.

The calculation results are shown in Figs. 3 and 4.

The modelling results (highlighted by boxes and arrows in Figs. 3 and 4) indicate that the minimum cod-end diameter at T0 orientation is 21.6 mm, which is smaller than the diameter at T90 orientation (29.0 mm). Visually, the area of tapering is shorter for T90 than for T0. Thus, the results obtained using the authors mathematical model agree with those from a field experiment in a hydro-channel.

Table 2. Parameters of external influence

№	Parameter	Designation	Value
1	Trawling speed	v	2 m/s
2	Water density	ρ	1030 кg/m^3
3	Kinematic viscosity of water	υ	1,004 mm^2/s
4	Catch volume	V	500 cm^3

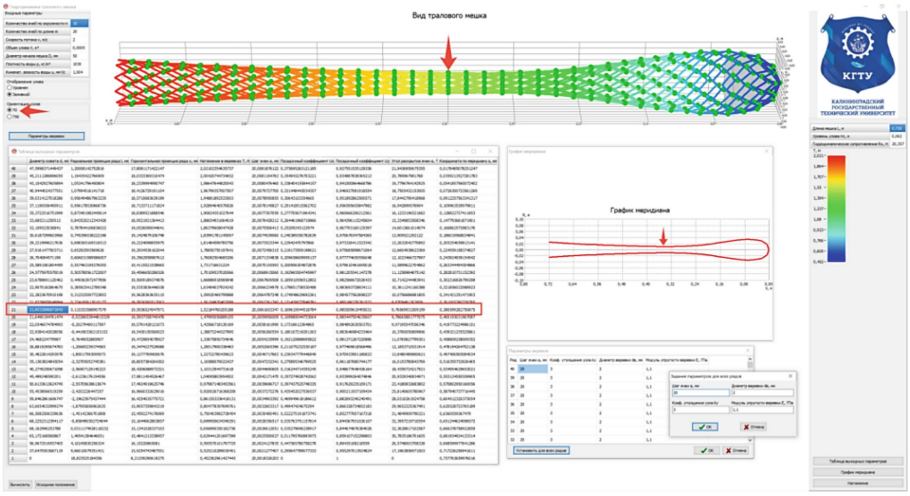

Fig. 3. Numerical simulation of the trawl cod-end with T0 mesh orientation

Methods based on heuristic relationships for hydrodynamic characteristics are suitable only for steady-state trawling. To assess transitional processes, a full Navier-Stokes hydrodynamic calculation is required.

The objective is to determine the hydrodynamic fields through mathematical modeling of the net-engineering construction, exemplified by a trawl cod-end. Assuming that the density of the net components and the catch is comparable to the density of the surrounding fluid (a reasonable assumption for a trawl cod-end), the hydrodynamic drag forces will substantially exceed the hydrostatic forces. In normal operation, the velocity vector of the trawl cod-end displacement is parallel to its axis. Under these conditions, hydrostatic forces can be neglected, allowing the problem to be reduced to a two-dimensional coordinate system, thereby decreasing computational effort and expediting the modeling process and result acquisition.

For the solution of hydrodynamic problems there exist various approaches, such as the pressure-velocity method and the stream-function method. The advantages of the stream-function method over the pressure-velocity method are as follows:

1. automatic enforcement of the incompressibility condition of the fluid;

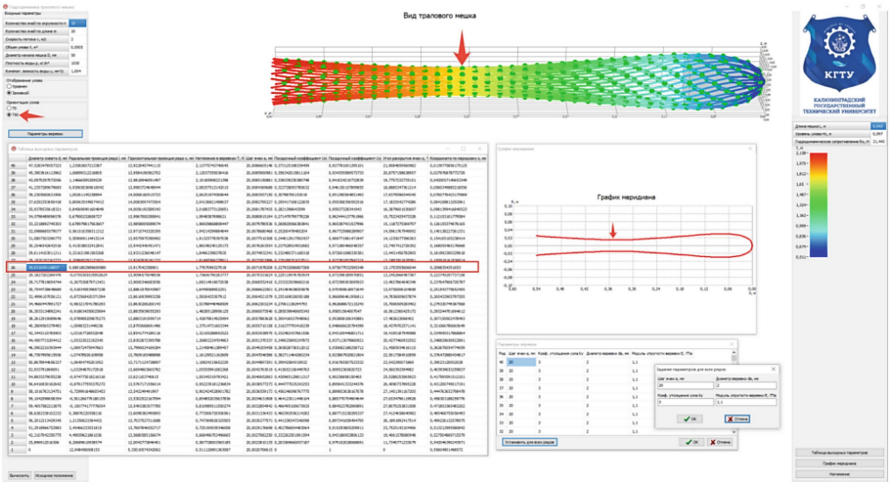

Fig. 4. Numerical simulation of the trawl cod-end with T90 mesh orientation

2. absence of pressure in the governing equations, and consequently no need for pressure boundary conditions;
3. reduction in the number of equations – instead of three equations in the pressure-velocity approach for a two-dimensional formulation, only two equations are solved;
4. ease of visualization – lines of constant stream-function value are streamlines of the fluid, making the stream-function an ideal tool for visualizing flow structure; the vorticity field clearly delineates regions of fluid rotation and the presence of vortices.

We introduce a Cartesian computational coordinate system Oxy. The Ox axis is directed to the right, along the symmetry axis of the net structure, while the Oy axis points upward from the symmetry axis. Figure 5 illustrates the coordinate system used for the calculation of the trawl cod-end.

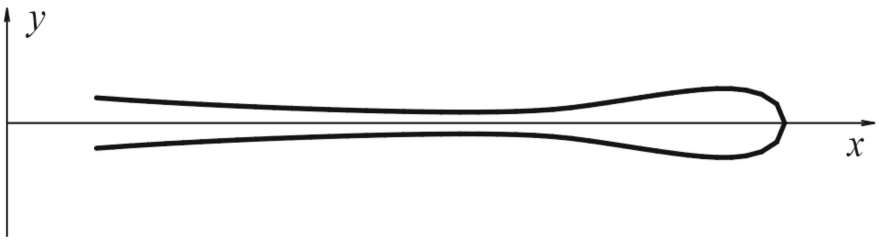

Fig. 5. The coordinate system

In the vorticity-stream function method (hereafter ω-ψ method), the concepts of vorticity field ω and stream function ψ are introduced:

$$\omega = \frac{\partial v_y}{\partial x} - \frac{\partial v_x}{\partial y},$$

$$v_x = \frac{\partial \psi}{\partial y}, v_y = -\frac{\partial \psi}{\partial x},$$

where v_x, v_y – are the projections of the fluid velocity onto the Oxy plane along the coordinate axes.

Let us write the continuity and Navier-Stokes equations for an incompressible viscous fluid in vector form.

$$\nabla \mathbf{g} \boldsymbol{v} = 0,$$

$$\frac{\partial \boldsymbol{v}}{\partial t} + (\boldsymbol{v}\mathbf{g}\nabla)\boldsymbol{v} = -\frac{1}{\rho}\nabla p + \nu \nabla^2 \boldsymbol{v},$$

where $\mathbf{v}$ – is the velocity vector of the fluid at an arbitrary point in space (for the two-dimensional case the plane Oxy); t – is time; ρ – is the fluid density; p – is the pressure at an arbitrary point in fluid (for the two-dimensional case the plane Oxy); ν – is the kinematic viscosity of the fluid.

$$\frac{\partial v_x}{\partial x} + \frac{\partial v_y}{\partial y} = 0,$$

$$\frac{\partial v_x}{\partial t} + v_x \frac{\partial v_x}{\partial x} + v_y \frac{\partial v_x}{\partial y} = \nu \left(\frac{\partial^2 v_x}{\partial x^2} + \frac{\partial^2 v_x}{\partial y^2} \right) - \frac{1}{\rho} \frac{\partial p}{\partial x}.$$

By differentiating with respect to y and x respectively (and taking the appropriate terms into account), we obtain the Helmholtz equation.

$$\frac{\partial \omega}{\partial t} + v_x \frac{\partial \omega}{\partial x} + v_y \frac{\partial \omega}{\partial y} = \nu \left(\frac{\partial^2 \omega}{\partial x^2} + \frac{\partial^2 \omega}{\partial y^2} \right).$$

And the Poisson equation

$$\frac{\partial^2 \psi}{\partial x^2} + \frac{\partial^2 \psi}{\partial y^2} = -\omega.$$

As initial conditions for the velocity, vorticity and stream function fields we will assume.

$$vx = vw, vy = 0, \omega = 0,$$

$\psi(y) = \int v_w dy$, $\psi(0) = 0$,

where v_w – is the prescribed inflow velocity of the fluid.

We prescribe the boundary conditions: at the boundaries of the computational grid, we impose a first-kind (Dirichlet) condition for vorticity and a second-kind (Neumann) condition for the stream function:

$$\omega = 0,$$

$\frac{\partial \psi}{\partial y} = v_x$ - on the left and right boundaries,
$\frac{\partial \psi}{\partial x} = -v_y$ - on the top and bottom boundaries.
On the surface of an impermeable wall, we apply the generalized Thomson condition:

$$\omega_b = -\frac{\partial^2 \psi}{\partial \boldsymbol{n}^2},$$

where ω_b – is the vorticity on the fully impermeable wall; **n** – is the outward normal vector to the surface directed away from the grid structure. Considering the continuity of the grid surface F_O, the boundary condition can be rewritten as:

$$\omega = F_O \omega_b + \omega_w,$$

where ω_w – vorticity in fluid.

The vorticity field is obtained analogously to solving the Navier-Stokes equations by the «pressure-velocity» method. Using an implicit finite-difference approximation on a regular grid with step h Ox and Oy and the splitting method, each time step k is divided into two sub-steps. The first equation is along axis Ox, the second along axis Oy:

$$\frac{\omega^{\langle k+\frac{1}{2}\rangle} - \omega^{\langle k\rangle}}{\tau} = -v_x \left(\frac{\partial \omega}{\partial x}\right)^{\langle k+\frac{1}{2}\rangle} + \nu \left(\frac{\partial^2 \omega}{\partial x^2}\right)^{\langle k+\frac{1}{2}\rangle},$$

$$\frac{\omega^{\langle k+1\rangle} - \omega^{\langle k+\frac{1}{2}\rangle}}{\tau} = -v_y \left(\frac{\partial \omega}{\partial y}\right)^{\langle k+1\rangle} + \nu \left(\frac{\partial^2 \omega}{\partial y^2}\right)^{\langle k+1\rangle},$$

where

$$v_x \left(\frac{\partial \omega}{\partial x}\right)^{\langle k+\frac{1}{2}\rangle} = \frac{\left(v_{xi,j} + \left|v_{xi,j}\right|\right)\left(\omega_{i,j}^{\langle k+\frac{1}{2}\rangle} - \omega_{i-1,j}^{\langle k+\frac{1}{2}\rangle}\right) + \left(v_{xi,j} - \left|v_{xi,j}\right|\right)\left(\omega_{i+1,j}^{\langle k+\frac{1}{2}\rangle} - \omega_{i,j}^{\langle k+\frac{1}{2}\rangle}\right)}{2h},$$

$$v_y \left(\frac{\partial \omega}{\partial y}\right)^{\langle k+1\rangle} = \frac{\left(v_{yi,j} + \left|v_{yi,j}\right|\right)\left(\omega_{i,j}^{\langle k+1\rangle} - \omega_{i,j-1}^{\langle k+1\rangle}\right) + \left(v_{yi,j} - \left|v_{yi,j}\right|\right)\left(\omega_{i,j+1}^{\langle k+1\rangle} - \omega_{i,j}^{\langle k+1\rangle}\right)}{2h},$$

$$\left(\frac{\partial^2 \omega}{\partial x^2}\right)^{\langle k+\frac{1}{2}\rangle} = \frac{\omega_{i-1,j}^{\langle k+\frac{1}{2}\rangle} - 2\omega_{i,j}^{\langle k+\frac{1}{2}\rangle} + \omega_{i+1,j}^{\langle k+\frac{1}{2}\rangle}}{h^2},$$

$$\left(\frac{\partial^2 \omega}{\partial y^2}\right)^{\langle k+1\rangle} = \frac{\omega_{i,j-1}^{\langle k+1\rangle} - 2\omega_{i,j}^{\langle k+1\rangle} + \omega_{i,j+1}^{\langle k+1\rangle}}{h^2},$$

k – the step number.

Indices of fractional steps are denoted within angle brackets.

The velocity field is obtained from the stream-function field using a finite-difference scheme:

$$v_{xi,j} = \frac{\psi_{i+1,j} - \psi_{i-1,j}}{2h},$$

$$v_{yi,j} = \frac{\psi_{i,j+1} - \psi_{i,j-1}}{2h}.$$

To compute the vorticity field at each fractional time step, one must solve a system of linear algebraic equations (SLAE).

$$\boldsymbol{A\omega} = \boldsymbol{d},$$

where **A** – the coefficient matrix for the unknown vector-column **ω**; **d** – the right-hand-side vector-column.

Since the matrix **A** is tridiagonal, the resulting SLAE can be solved by the Thomas algorithm (method of elimination). In the forward sweep for $i = [1\ldots n]$ we obtain.

$\delta_i = -a_{i,i+1}/\left(a_{i,i} + a_{i,i-1}\delta_{i-1}\right)$, $\beta_i = \frac{(d_i - a_{i,i-1}\beta_{i-1})}{(a_{i,i} + a_{i,i-1}\delta_{i-1})}$,

where β and δ – temporary variables; $\beta_0 = 0$, $\delta_0 = 0$, $a_{1,i\text{-}1} = 0$, $a_{n,i+1} = 0$; n – the number of nodes in the computational grid along the considered directions *Ox* and *Oy*.

In the backward sweep for $i = [n\ldots 1]$ we obtain:

$$\omega_i = \delta_i \omega_{i+1} + \beta_i$$

where $\omega_{n+1} = 0$**.**

To compute the vorticity field, the Poisson equation must be solved. For this purpose, the Richardson or Libman numerical methods with upper relaxation are employed. The Richardson method, unlike the Libman method, requires an intermediate data array but is easily parallelizable. The Libman method requires updating the intermediate values of the unknown quantity immediately after they are computed at each step of the successive approximation, but it converges faster when performed sequentially. Consequently, in heterogeneous computing systems we use both methods: the first for computations on a graphics processing unit (GPU) and the second on a central processing unit (CPU). Below are finite-difference schemes for the Richardson method

$$\psi_{i,j}^{\langle k+1\rangle} = \frac{1}{4}\left(\psi_{i+1,j}^{\langle k\rangle} + \psi_{i-1,j}^{\langle k\rangle} + \psi_{i,j+1}^{\langle k\rangle} + \psi_{i,j-1}^{\langle k\rangle} + h^2\omega_{i,j}\right)$$

and for the Libman method with upper relaxation:

$$\psi_{i,j}^{\langle k+1\rangle} = (1-\theta)\psi_{i,j}^{\langle k\rangle} + \frac{\theta}{4}\left(\psi_{i+1,j}^{\langle k\rangle} + \psi_{i-1,j}^{\langle k+1\rangle} + \psi_{i,j+1}^{\langle k\rangle} + \psi_{i,j-1}^{\langle k+1\rangle} + h^2\omega_{i,j}\right),$$

where θ – a constant that influences the convergence speed of the algorithm.

Good results are obtained when:

$$\theta = \frac{1}{2\xi^2}\left(1 - \sqrt{1-\xi^2}\right), \xi = \frac{1}{2}\left(cos\frac{\pi}{n_x} + cos\frac{\pi}{n_y}\right),$$

where n_x, n_y – dimensions of the computational grid; ξ – an intermediate variable.

Let us write the termination condition of the iterative process when solving the Poisson equation:

$$max\left|\psi_{i,j}^{\langle k+1\rangle} - \psi_{i,j}^{\langle k\rangle}\right| < \varepsilon_\psi,$$

where ε_ψ – denotes the prescribed maximum error of the stream function.

The calculation of the convergence condition requires sequential accesses to a variable that holds the current error. For CPU-based computations, this issue does not arise. For GPU-based computations, where many computational blocks execute the same algorithm, it is necessary to prevent simultaneous updates of the variable containing the current error. This can be achieved using a parallel-reduction algorithm with shared memory. The core idea is to partition the entire computational grid into blocks, which are in turn subdivided into nested blocks. The maximum-error search is performed sequentially within each block, while the blocks are processed in parallel over time. In the resulting search tree, nesting levels are processed sequentially from leaves to root. Each nested block maintains its own variable for the current error, whose value is passed to the next level. The process repeats until the root of the tree is reached.

When solving the Poisson equation on a GPU, a simplified algorithm that does not require computing the maximum error can be used. Its essence lies in creating an outer loop with a fixed number of iterations. The drawback of this algorithm is the lack of error control; reducing the error requires increasing the number of loops, which can lead to redundant computations.

The hydrodynamic drag force vector $\mathbf{R}$ of the net structure is given by the following expression:

$$\boldsymbol{R} = \boldsymbol{R}_p + \boldsymbol{R}_f, \boldsymbol{R}_p = \iint_S F_O p\, \boldsymbol{n} ds, \boldsymbol{R}_f = \iint_S F_O \rho \nu \frac{d\boldsymbol{v}_s}{d\boldsymbol{n}} ds,$$

where $\mathbf{R}_\mathrm{p}$ – fluid pressure force acting on the structure; $\mathbf{R}_\mathrm{f}$ – fluid friction force acting on the structure; S – surface of the net-engineering construction; $\mathbf{n}$ – unit normal vector to an infinitesimal surface element ds, directed outward from the structure; $\mathbf{v}_\mathrm{s}$ – projection of the velocity vector onto the plane parallel to the infinitesimal surface element ds.

4 Conclusion

The present work demonstrates that hydrodynamic backwater is a decisive factor governing the catch-efficiency of trawl cod-ends in open-water fisheries. By integrating a robust ω-ψ numerical scheme with experimental validation, we quantified how design variables – particularly inlet diameter, mesh spacing, and mesh orientation – modulate pressure differentials within the net. The identified optimal configuration (minimum inlet diameter, reduced mesh spacing, T90 mesh orientation) achieves a significant reduction in hydrodynamic backwater and a corresponding increase in catch-efficiency, offering a practical pathway for net manufacturers and fishers to improve gear performance.

Furthermore, the analysis reveals a clear trade-off between trawling speed and hydrodynamic backwater: speeds exceeding 2.5 m/s lead to excessive pressure differences that

facilitate fish escape, thereby diminishing efficiency. Maintaining trawling speeds within the 1.5–2.5 m/s window balances throughput and retention.

The alignment of computational results with hydro-channel data validates the ω-ψ approach as a reliable tool for predicting hydrodynamic behavior of fishing gear. Future work should explore adaptive net designs that dynamically adjust mesh spacing or mesh orientation in response to real-time flow conditions, potentially leveraging machine-learning control systems.

In summary, incorporating hydrodynamic backwater considerations into trawl codend design yields measurable performance gains and enhances the sustainability of trawl fisheries by optimizing catch rates while minimizing environmental impact.

Acknowledgements. The research was conducted at the Kaliningrad State Technical University with funding from the Russian Science Foundation grant No 25-21-00008, https://rscf.ru/project/25-21-00008/.

References

1. Graham, N., O'Neill, F.-G., Fryer, R.-J., Galbraith, R.-D., Myklebust, A.: Selectivity of a 120 mm diamond codend and the effect of inserting a rigid grid or a square mesh panel. Fish. Res. **67**(2), 151–161 (2004). https://doi.org/10.1016/j.fishres.2003.09.037
2. Herrmann, B., Wienbeck, H., Moderhak, W., Stepputtis, D., Krag, L.-A.: The influence of twine thickness, twine number and netting orientation on codend selectivity. Fish. Res. **145**, 22–36 (2013). https://doi.org/10.1016/j.fishres.2013.03.002
3. Moderhak, W.: A theoretical approach to selectivity of cod-ends. Contrib. Theory Fish. Gears Related Marine Syst. **3**, 105 (2003)
4. Herrmann, B., Priour, D., Krag, L.-A.: Simulation-based study of the combined effect on cod-end size selection of turned meshes by 90 and reducing the number of meshes in the circumference for round fish. Fish. Res. **84**(2), 222–232 (2007). https://doi.org/10.1016/j.fishres.2006.10.020
5. Digre, H., Hansen, U.-J., Erikson, U.: Effect of trawling with traditional and 'T90'trawl codends on fish size and on different quality parameters of cod Gadus morhua and haddock Melanogrammus aeglefinus. Fish. Sci. **76**(4), 549–559 (2010). https://doi.org/10.1007/s12562-010-0254-2
6. Razhev, A.-O.: Mechanics of Net-Based Fishing Gear for Inland and Coastal Fisheries. Dissertation for the degree of Candidate of Technical Sciences, p. 201 (2020)
7. Nedostup, A.-A.: Methods of Calculating Net-Based Passive Fishing Gear for Inland and Coastal Fisheries, p. 281. Kaliningrad State Technical University, Kaliningrad (2010)
8. Idelchik, I.-E.: Handbook of Hydraulic Resistances. 4th ed., revised and expanded, p. 672. Mashinostroenie, Moscow (1992)
9. Hoerner, S.-F.: Fluid-Dynamic Drag: Practical Information on Aerodynamic Drag and Hydrodynamic Resistance, p. 455. Bricktownship (1965)